Supporting Information for

From relaxation to buckling: A continuum elastic framework connecting surface instabilities of highly compressed lipid thin films

Anna D. Gaffney, Dongxu Liu, Deepanjali Samal, Angelo R. Carotenuto, Luca Deseri, Massimiliano Fraldi, Ka Yee C. Lee, Luka Pocivavsek, and Nhung Nguyen

Anna Gaffney
E-mail: adgaffney@uchicago.edu
Nhung Nguyen
E-mail: nhungng@uchicago.edu

This PDF file includes:

Supporting text
Figs. S1 to S2
Legends for Movies S1 to S3
SI References

Other supporting materials for this manuscript include the following:

Movies S1 to S3

Supporting Information Text

1. Constitutive Model Implementation.

Basic Kinematics. A lipid monolayer is assumed to be a continuum body. Consider an arbitrary material particle in the reference configuration $\mathcal{B}_0$ of the continuum body at the reference time $t = 0$. The position of the particle is characterized by its position vector $\mathbf{X}$. This particle transforms to a position $\mathbf{x}$ in the current configuration $\mathcal{B}$ at time t following the motion $\chi(\mathbf{X}, t)$. The deformation gradient tensor is defined as $\mathbf{F} \coloneqq \partial\mathbf{x}/\partial\mathbf{X}$. The determinant of $\mathbf{F}$ is denoted by $J \coloneqq det\mathbf{F} > 0$. The right and left Cauchy–Green deformation tensors are introduced as $\mathbf{C} \coloneqq \mathbf{F}^T\mathbf{F}$ and $\mathbf{B} \coloneqq \mathbf{F}\mathbf{F}^T$, respectively. The spatial velocity gradient tensor is given as $\mathbf{L} \coloneqq \dot{\mathbf{F}}\mathbf{F}^{-1}$, with $(\dot{\bullet})$ the material time derivative of a quantity $(\bullet)$. $\mathbf{F}$ is split into an isochoric part $J^{1/3}\mathbf{I}$ and a volumetric part $\overline{\mathbf{F}}$, i.e., $\mathbf{F} = J^{1/3}\overline{\mathbf{F}}$, where $\mathbf{I}$ is the 2nd-order identity tensor, and $\overline{\mathbf{F}}$ is the modified deformation gradient tensor. Thus, the modified right and left Cauchy–Green deformation tensors are correspondingly introduced as $\overline{\mathbf{C}} \coloneqq \overline{\mathbf{F}}^T\overline{\mathbf{F}}$ and $\overline{\mathbf{B}} \coloneqq \overline{\mathbf{F}}\overline{\mathbf{F}}^T$, respectively.

Constitutive Relations. The Helmholtz free energy density function ψ is assumed to exist, which is defined per unit reference volume. Within the large deformation framework, the free energy density is assumed to be a function of the right Cauchy–Green deformation tensor, i.e., $\psi = \hat{\psi}(\mathbf{C})$. In this work, we focus on the experimental state where a lipid monolayer exhibits the solid phase, where the monolayer shows quasi-incompressible characteristics. To separately describe the isochoric and volumetric contributions, the free energy density ψ is decomposed into two parts, i.e.,

$$\psi = \psi_{iso} + \psi_{vol}, \text{with } \psi_{iso} = \hat{\psi}_{iso}(\bar{\mathbf{C}}) \text{ and } \psi_{vol} = \hat{\psi}_{vol}(J), \tag{1}$$

where $\overline{\mathbf{C}}$ and J can be expressed as functions of $\mathbf{C}$, i.e., $\overline{\mathbf{C}} = J^{-2/3}\mathbf{C}$ and $J = (det\mathbf{C})^{1/2}$, respectively.

Under the isothermal conditions, the Clausius–Planck inequality is expressed as

$$\mathcal{D}_{int} = \mathbf{S} \cdot \frac{\dot{\mathbf{C}}}{2} - \dot{\psi} = \left(\mathbf{S} - 2\frac{\partial\psi}{\partial\mathbf{C}}\right) \cdot \frac{\dot{\mathbf{C}}}{2} \geq 0, \tag{2}$$

where $(\bullet) \cdot (\bullet)$ denotes a double contraction, $\mathbf{S}$ represents the second Piola–Kirchhoff stress tensor, and $\mathcal{D}_{int}$ is the non-negative internal dissipation. Since $\mathbf{C}$ can be chosen arbitrarily, to fulfill the inequality, one has

$$\mathbf{S} = 2\frac{\partial\psi}{\partial\mathbf{C}}. \tag{3}$$

The Cauchy stress σ can be calculated as

$$\sigma = \frac{1}{J}\mathbf{F}\mathbf{S}\mathbf{F}^T = \frac{2}{J}\mathbf{F}\frac{\partial\psi}{\partial\mathbf{C}}\mathbf{F}^T. \tag{4}$$

Constitutive Relation in Simple Shear. For describing the shear banding of monolayers, a new invariant is defined to measure the amount of shear strain in simple shear (see (1) for more details), i.e.,

$$\gamma_S{}^2 = \overline{I}_1 - 3. \tag{5}$$

The free energy density can be rewritten as a function of γ and J, i.e., $\psi = \hat{\psi}(\gamma, J)$. The shear stress in simple shear is calculated as

$$\tau = \frac{\partial\psi}{\partial\gamma} = \frac{\partial\psi}{\partial\bar{I}_1}\frac{\partial\bar{I}_1}{\partial\gamma} = 2\gamma\frac{\partial\psi}{\partial\bar{I}_1}\ . \tag{6}$$

2. Tunability of Non-Monotonic Material Model. Taking the model described in the Methods, the shear stress-strain relationship in simple shear can be calculated through Eq S6 (where $\tau(\gamma)$ is stress in simple shear as a function of γ_S, the amount of shear strain in simple shear), which can be derived as

$$\tau(\gamma_S) = 2\gamma_S\frac{\partial\psi}{\partial\bar{I}_1} = 2\gamma\left[\frac{C_1}{1 + C_2\gamma_S{}^2} - \frac{C_1C_2\gamma_S{}^2}{(1 + C_2\gamma_S{}^2)^2} + 2C_3\gamma_S{}^2\right], \tag{7}$$

We have chosen three parameter sets to act as typical cases for this model (Case 1: $C_1 = 1$, $C_2 = 5$, $C_3 = 0.5$; Case 2: $C_1 = 1$, $C_2 = 5$, $C_3 = 0.1$; Case 3: $C_1 = 1$, $C_2 = 10$, $C_3 = 0.001$) as well as a neo-Hookean case ($C_1 = 1$, $C_2 = 0$, $C_3 = 0$), results for all of which are shown in Fig. 3. These cases were chosen to best showcase the range of behavior this model can capture. In Cases 2 and 3, there are inflection points where the shear stress-strain relationship in simple shear changes sign, giving a local maximum that is not given in Case 1 or the neo-Hookean case. Cases 2 and 3 differ in their critical shear strain value and in the extent of their relaxation regimes. Specifically, the second elastic regime is not exhibited within the given strain range for Case 3.

3. Comparison of Analytical and Numerical Loss of Ellipticity. The results of the loss of ellipticity calculation from Eq 6 for all typical cases with a $\gamma_{S,C}$ are shown in the subplots of Fig. 3. The $\lambda_{N,C}$ values for Case 2 and Case 3 are 0.874 and 0.914, respectively. Using the homogeneous FE model built with the constitutive equation as described in the Methods, we characterize the effective behavior of the material through recording reaction force on the left boundary as a function of nominal stretch, λ_N. The point where the reaction force drops is the critical nominal stretch, or $\lambda_{N,C}$. As shown in Fig. 3, this computational critical point agrees with the analytical onset of relaxation, suggesting the constitutive model can accurately capture the deformation of the matrix with different material properties. For the parameter sets that do not analytically provide a relaxation point, such as Case 1 and neo-Hookean, the results show no drop in reaction force, showcasing the ability for the analytical solution to differentiate between relaxation and no relaxation.

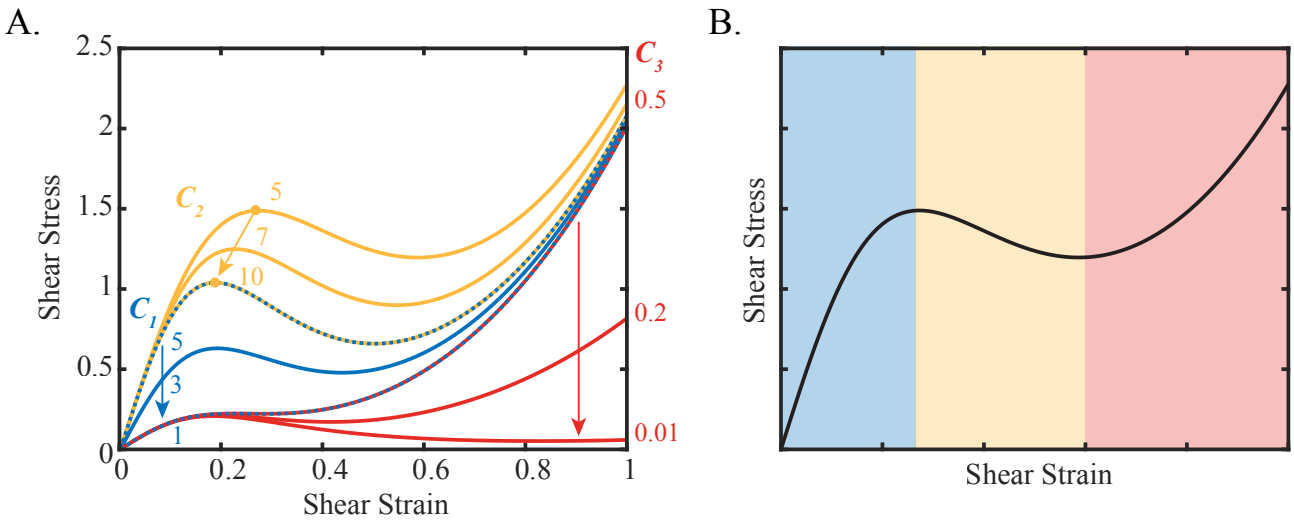

Fig. S1. Depiction of tunability and 3-regime form of shear banding material model. A) The shear stress-strain relationship in the case of simple shear is plotted for 7 different parameter sets to showcase the tunability of the chosen constitutive model, using Eq S7. C_1 (blue) is shown to alter the slope of the first elastic regime. C_2 (yellow) is shown to alter the critical shear strain or point of relaxation. C_3 (red) is shown to alter the slope of the second elastic regime. B) The shear stress-strain relationship in the case of simple shear is plotted for a representative parameter set to showcase the 3-regime form of the model when it is non-monotonic. The first region (blue) is considered the first elastic regime. The second region (yellow) is considered the relaxation regime, the presence of which allows for shear banding to take place. The third region (red) is considered the second elastic regime. When a parameter set creates a monotonic relationship, there is no relaxation regime.

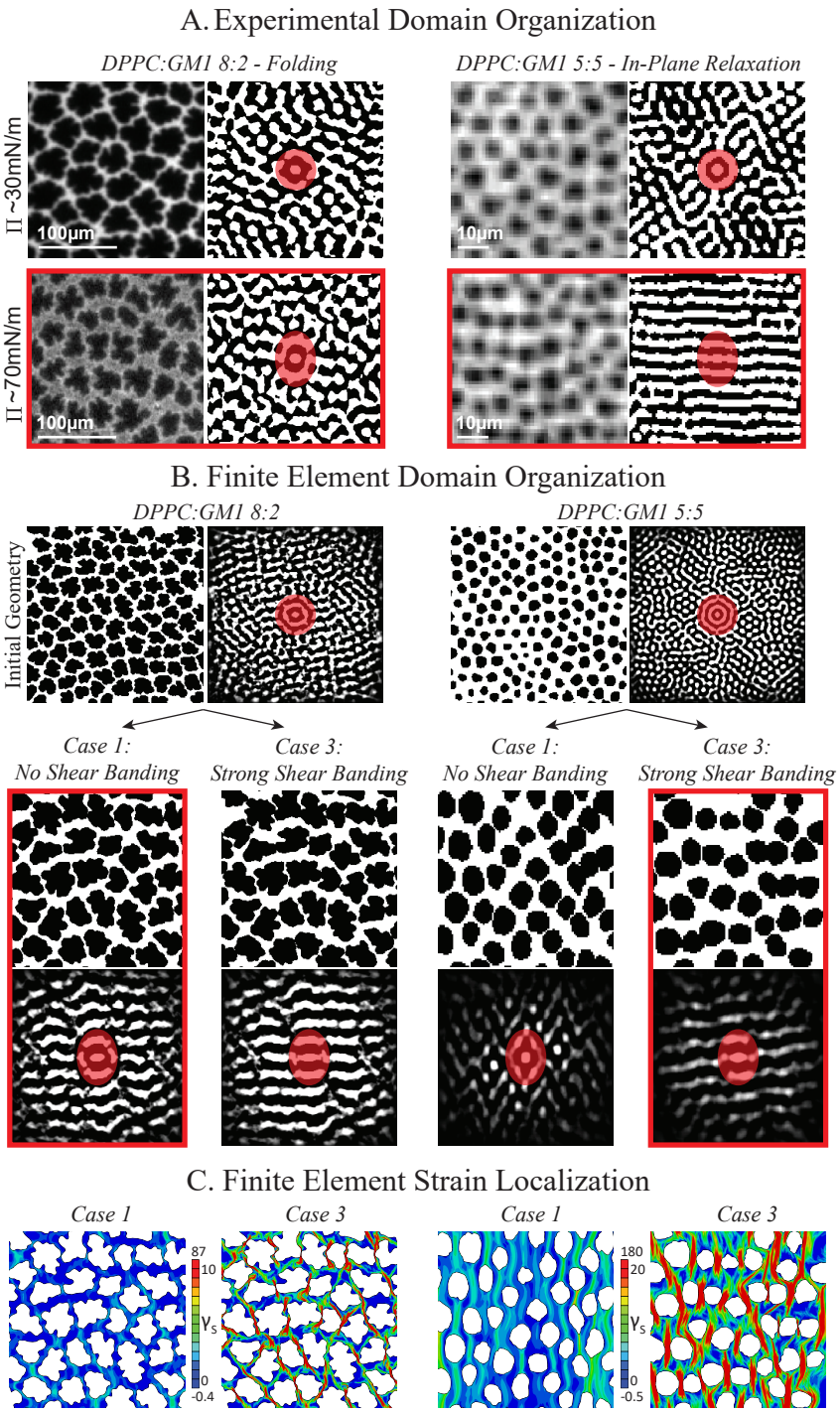

Fig. S2. Validation against additional lipid monolayer compositions. A) Evolution of representative local condensed domain organization captured by FM for monolayers that lose stability via folding (left, DPPC:G_{M1} 8:2) and relaxing in-plane (right, DPPC:G_{M1} 5:5) (further compositional details found in Method section) under increasing lateral compression, as previously published (2), with the associated 2D image autocorrelation to the right. These autocorrelations again show that for folding lipid monolayers, powder structure is maintained, while for in-plane relaxing monolayers, this powder structure is broken. B) Finite element resultant domain organization for an initial geometry of a folding monolayer (left, DPPC:G_{M1} 8:2) and monolayer that relaxes in-plane (right, DPPC:G_{M1} 5:5). For both models, Case 1 (no shear banding) shows maintained powder structure at high compression and Case 3 (strong shear banding) shows similar domain organization to that observed in in-plane relaxing monolayers. Red boxes enclose where the resultant FE model domain organization in B matches the experimental data in A. C) Representative field distributions of shear strain for resultant FE models shown in B. Significantly less localized shear strains are seen in models implementing a monotonic shear stress-strain response (Case 1), while strong shear bands form in the matrix for the non-monotonic shear stress-strain response, promoting condensed domain reorganization (Case 3).

Movie S1. The field distributions of shear strain (SDV), calculated using Eq S5, in the computational model where the matrix has the parameters of Case 1 (no shear banding), with strain limits adjusted to each frame, as shown in the legend.

Movie S2. The field distributions of shear strain (SDV), calculated using Eq S5, in the computational model where the matrix has the parameters of Case 2 (weak shear banding), with strain limits adjusted to each frame, as shown in the legend.

Movie S3. The field distributions of shear strain (SDV), calculated using Eq S5, in the computational model where the matrix has the parameters of Case 3 (strong shear banding), with strain limits adjusted to each frame, as shown in the legend.

References

1. W Seki, SN Atluri, Analysis of strain localization in strain-softening hyperelastic materials, using assumed stress hybrid elements. *Comput. Mech.* **14**, 549–585 (1994).
2. L Pocivavsek, et al., Lateral stress relaxation and collapse in lipid monolayers. *Soft Matter* **4**, 2019 (2008).